Assessment of Seismic and Magnetic Correlations

The overall approach is to compare, for each half day, seismic signatures in a sector in the far hemisphere spanning approximately 13.3° in longitude, i.e., one day times the mean synodic Carrington rotation rate (see Fig 1), with magnetic signatures ($|\mathbf{B}|$, $|B_r|$), in the region in the near hemisphere to which this sector will have rotated a few days thence, over a latitudinal range of ±60°.

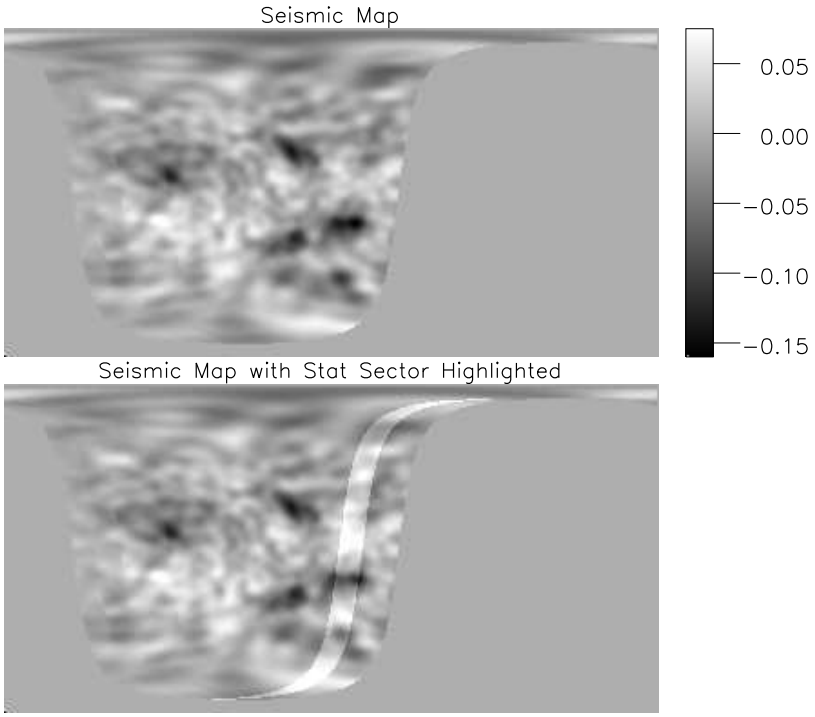

Figure 1. Map of a 1-day "reference sector" in the Sun's far hemisphere to be correlated with magnetic signatures to appear when visible from Earth. Top frame shows seismic map of the far hemisphere on 2011 March 20.0. Bottom frame shows the same with the reference sector whose center is two days before crossing the limb into direct view from Earth.

In order to make the comparisons with subsequent magnetic signatures, the Carrington-rotated seismic maps are to be projected onto the magnetic maps as viewed by HMI. This avoids interpolation errors, which are large for the high-resolution vector-magnetic maps and small for the low-resolution seismic maps, on account of their relative smoothness.

We make the comparisons in various latitudinal ranges ∼4 days after the date of the seismic maps, with control comparison 8.5 days after the seismic maps, when the reference sector is crossing the meridian in the near hemisphere. The control case is the easiest to show graphically, because the projection in the near hemisphere is spread over a greater area. This is shown in Figure 2.

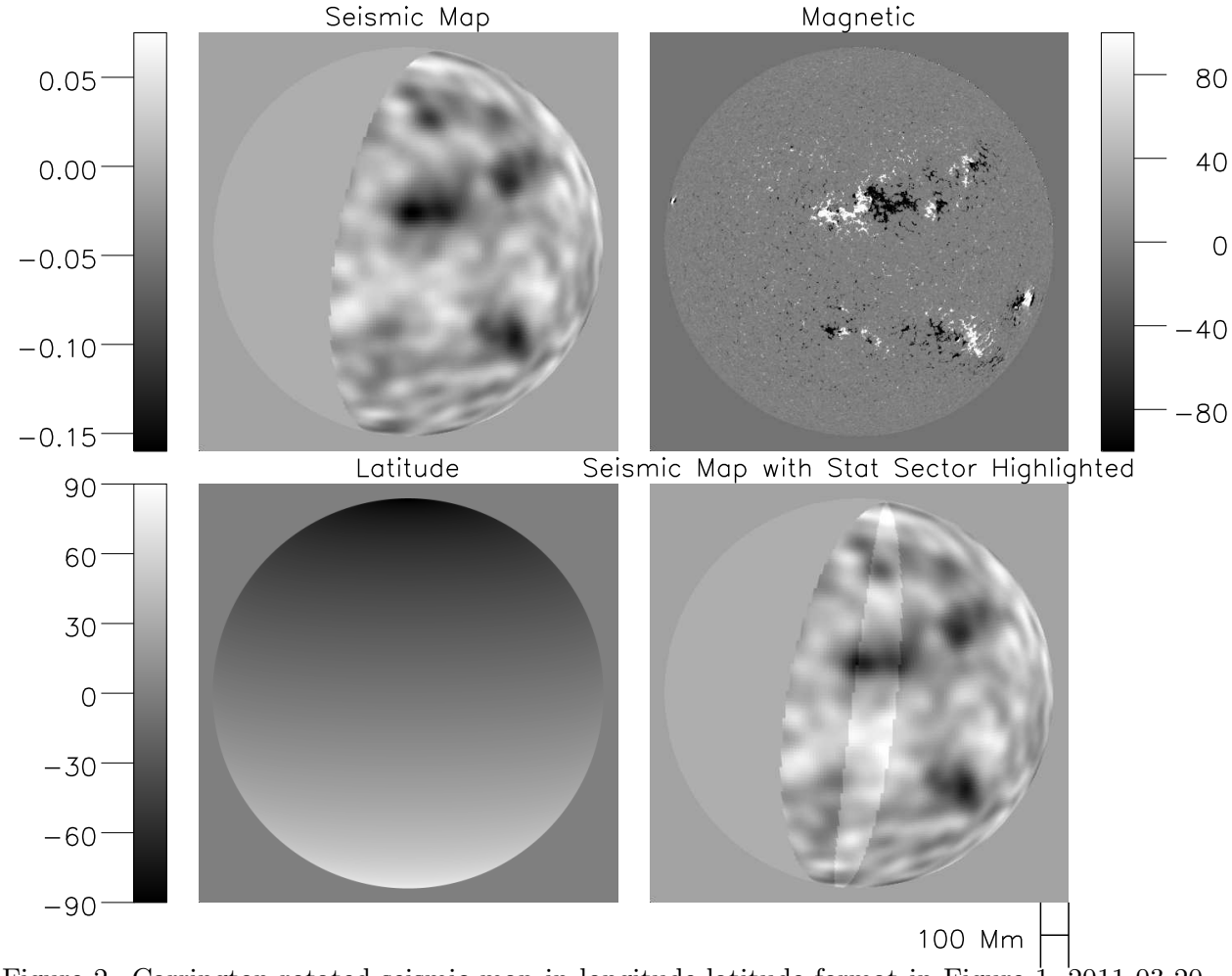

Figure 2. Carrington-rotated seismic map in longitude-latitude format in Figure 1, 2011-03-20 is projected onto SDO/HMI's view of the region in the near hemisphere 8.5 days thence (top left), i.e., at 2011-03-28.5. The HMI line-of-sight magnetogram for that moment is rendered in the top-right frame. A cospatial map of the latitude is shown at bottom left. Note that the image is inverted, with the north pole at the bottom of the image. Bottom right frame shows the seismic map with the reference sector highlighted.

The case for the 4-day delay (2011-03-24.0) from the reference date (2011-03-20.0) is shown in Figure 3. at this point the reference sector lies in a thin crescent just inside the Sun's eastern limb, at right in HMI's reference frame. A flick comparing the top two frames of Figure 2 is at `http://www.cora.nwra.com/ lindsey/public_html/NOAA_FarSide/FLICK01.gif`

The advantage of the correlations with a 4-day delay is that changes in the magnetic configuration—particularly those due to the emergence of new magnetic flux—are minimized. The advantage of the correlations with a 8.5-day delay is that errors in the radial component of the magnetic field are considerably reduced, as is loss of spatial discrimination due to foreshortening.

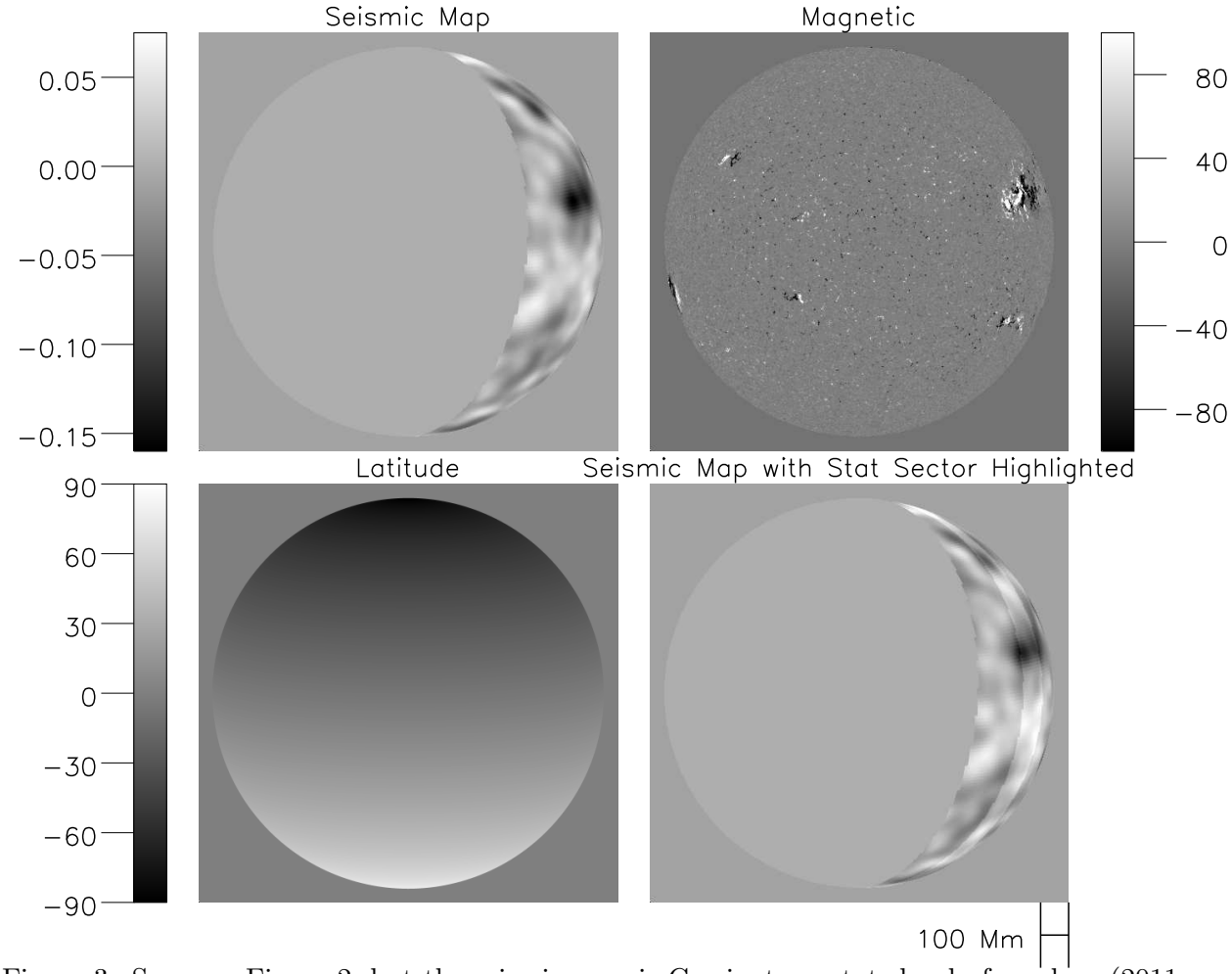

Figure 3. Same as Figure 2, but the seismic map is Carrington-rotated only four days (2011-03-24.0) from the reference date (2011-03-20.0), at which point the reference sector lies in a thin crescent just inside the Sun's eastern limb (keeping in mind that the HMI map is oriented so that north is almost directly downward).

The "time-latitude" maps that come out of this exercise, spanning the years 2011 through 2015 are plotted on the following two pages. The maps for the seismic signatures are plotted on the next page. The maps for the magnetic signatures are plotted on the page after the next. A two-frame movie cospatially flickering these presentations can be accessed at
`http://www.cora.nwra.com/ lindsey/SeisMagFlick.gif`.

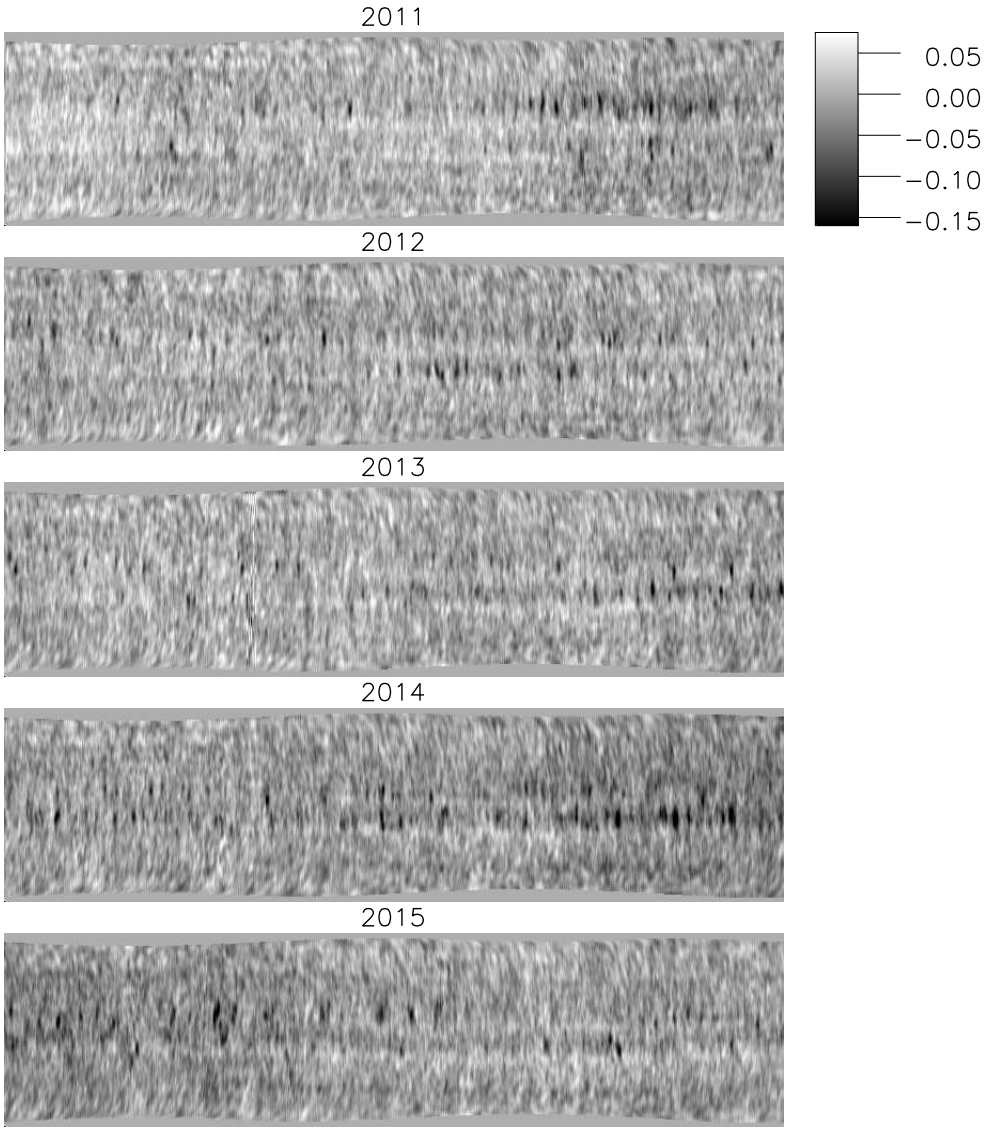

Figure 4. Time-latitude maps of the seismic signature passing through the strip in longitude highlighted in Figure 1 for one-year periods from 2011 (top panel) through 2015 (bottom). Time is represented linearly in the horizontal direction of each map, spanning a full year from left to right. Latitude is represented linearly in the vertical direction of each map, from the Sun's south pole (bottom) to the north pole (top). The gray scale represents the seismic signature as a phase shift in radians. Seismic signatures of large active regions appear as dark vertical exclamatory clefts in the active-region bands, i.e., the latitude range $\pm 30°$.

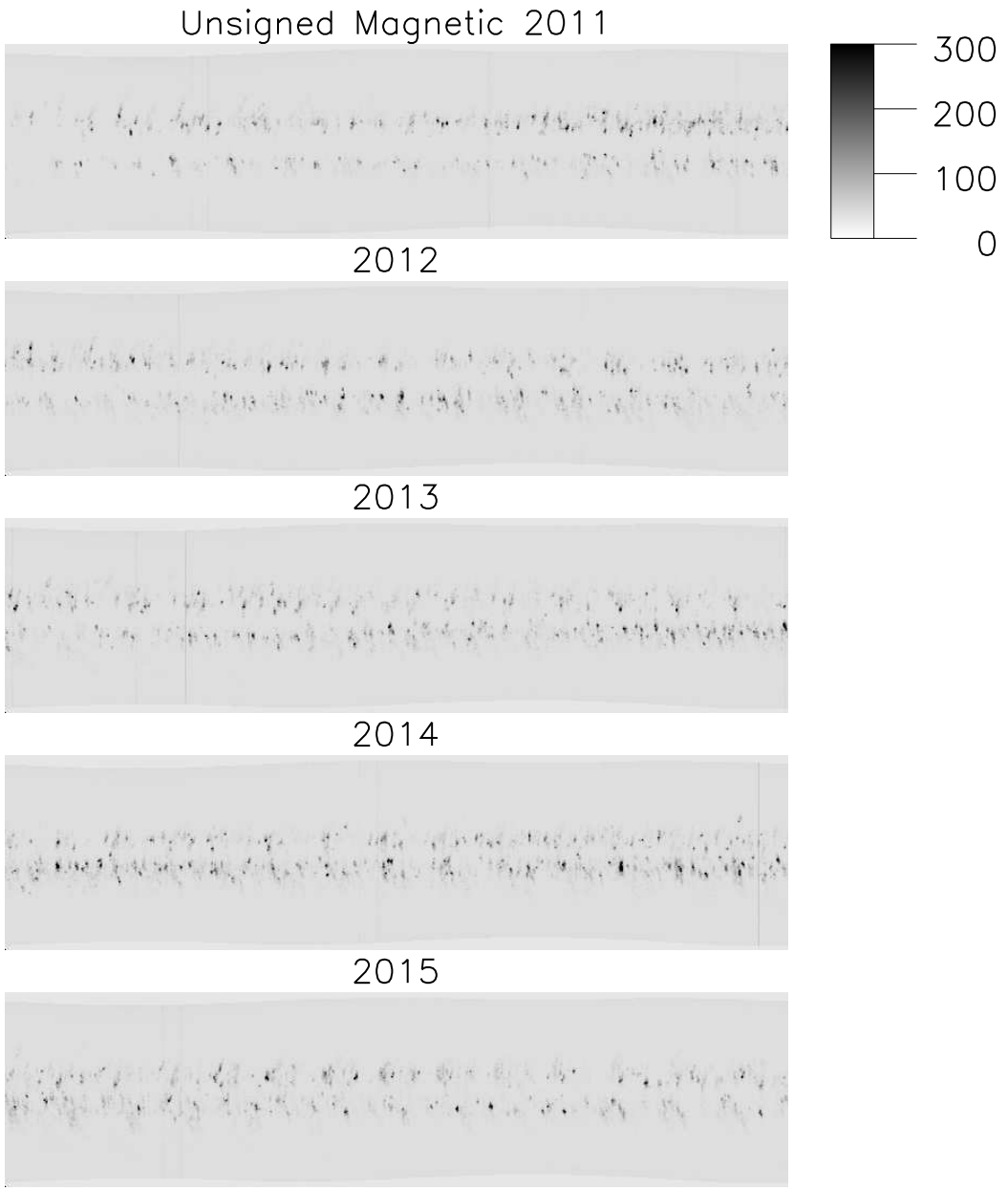

Figure 5. Time-latitude maps of the unsigned magnetic flux passing through the strip in longitude highlighted in Figure 1 for one-year periods from 2011 (top panel) through 2015 (bottom). As in Figure 4, above, with which this presentation is both cospatial and cotemporal, time is represented linearly in the horizontal direction of each map, spanning a full year from left to right. Latitude is represented linearly in the vertical direction of each map, from the Sun's south pole (bottom) to the north pole (top). The gray scale represents the seismic signature as a phase shift in radians. Large active regions appear as dark features.

Update of Assessment of Seismic and EUV Correlations

Paulett sent us high-quality FITS maps of HeI 304-Å intensity in Carrington-longitude-vs-latitude format to replace the ones Charlie crudely reconstructed from color-JPEG maps. The seismic strengths, S, plotted in Figure 1 of the Second Interim Report of active regions that reach a maximum relatively early in their transit of the far hemisphere tended to show large decreases following their maxima. It was recognized that this was largely due to the phase signature, ϕ, being integrated over an area that decreased with the seismic signature itself, since this area was that in which the seismic signature exceed a minimal threshold. To alleviate this decrease, we replaced the strengths published by the Stanford JSOC by integrals over the same elliptical regions over which we integrated the HeI 304-Å intensity. Several aspects of the relationship between the seismic signatures and EUV brightnesses are shown in the following four Figures:

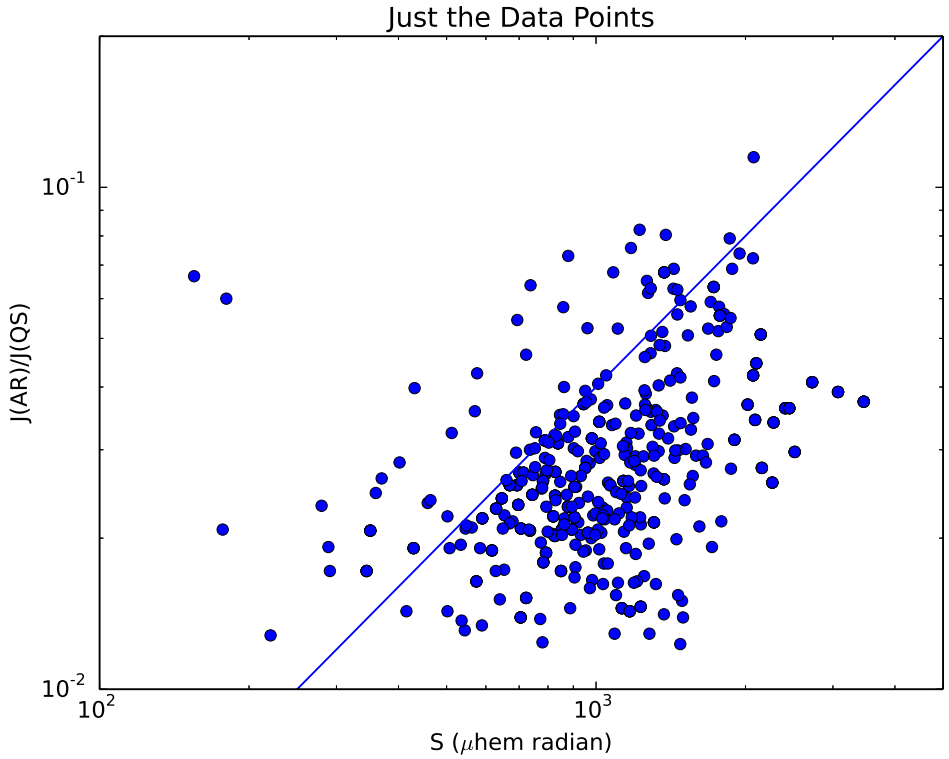

Figure 4. Scatter plot of seismic strengths, S (abscissa), and EUV radiances (J—normalized to the mean quiet Sun integrated over the near hemisphere—ordinate) Blue diagonal line shows linear eyeball fit of the precipice in the distribution of data points with a power-law exponent of unity.

Figure 4 shows a simple scatter plot of HeI 304-Å-brightness (ordinate) vs S (abscissa) for all of the seismic signatures in Intervals 1 (February through April of 2011) and 2 (January through April of 2012). The breadth of the distribution of these data points is considerable, about a half oder of magnitude proceeding rightward from the diagnonal

blue line, which marks an apparent precipice in the distribution. Charlie's guess is that the precipice is basically a manifestation of active regions that are already both strong and bright passing across the west limb into the far hemisphere. The data points to the left of the precipice predominantly represent active regions whose seismic signature have reached their maxima, and whose seismic signatures are decaying more rapidly faster than their brightnesses, notwithstanding that their seismic phases are now being integrated over the same, fully encompassing, region both as their EUV brightnesses.

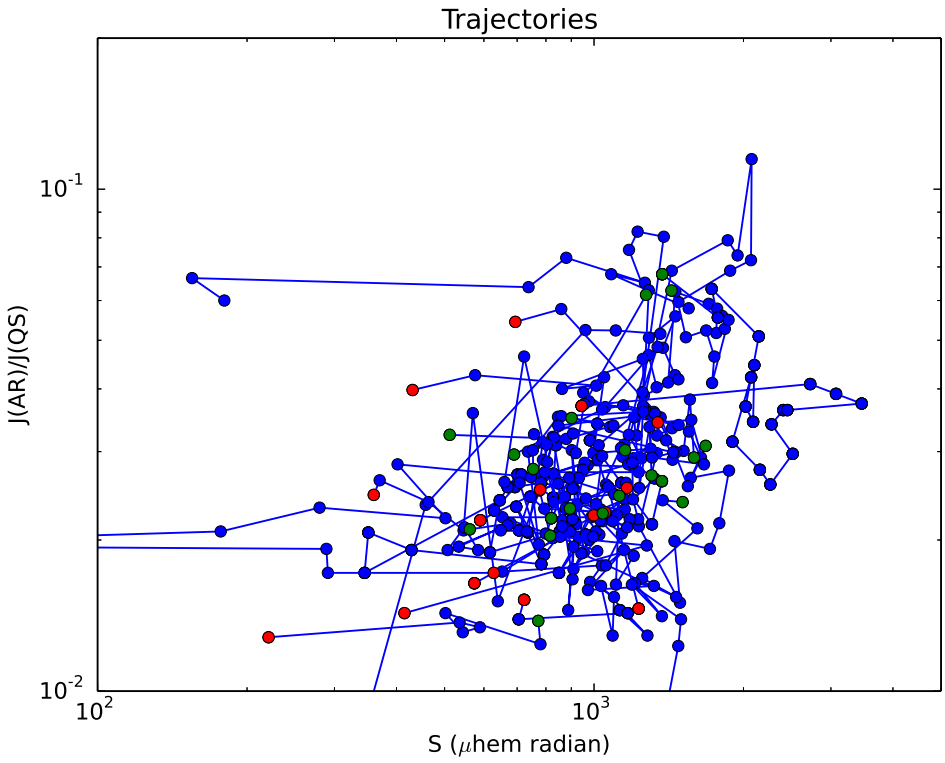

Figure 5. Trajectories of HeI 304-Å brightness, J, normalized to unity for a quiet solar hemisphere (ordinate) and strength, S, (abscissa) of the seismic signature for the 22 active regions whose seismic signatures were clearly detectable during Intervals 1 and 2. The beginning of each trajectory is colored green. The end point of each is colored red. All others are rendered in blue.

Figure 5 attempts to show the actual trajectories of the seismic signatures and respective EUV brightnesses. vs S for all of the seismic signatures in the time interval originally analyzed by Paulett (i.e., February through April of 2011 The green points show the starting points of the trajectories, while the red points show the end points. Four of the trajectories, 22 in all, are seen to end to the left of the precipice, their seismic signatures having decayed while their brightnesses have remained nearly constant.

Figure 6 shows only the data points at which the seismic signature is at its maximum. These data points fit a power-law profile,

$$S \;=\; S_0 J^{\gamma}, \tag{1}$$

(blue diagonal line), where

$$\begin{aligned} \gamma &= \frac{2}{5}, \text{ and} \\ S_0 &= 5742\ \mu\text{hem radian}, \end{aligned} \tag{2}$$

with an rms deviation of $(4/3)S$ to the right and $(3/4)S$, as indicated by the parallel diagonal green lines, where J for an entire solar hemisphere is normalized to unity for the quiet Sun.

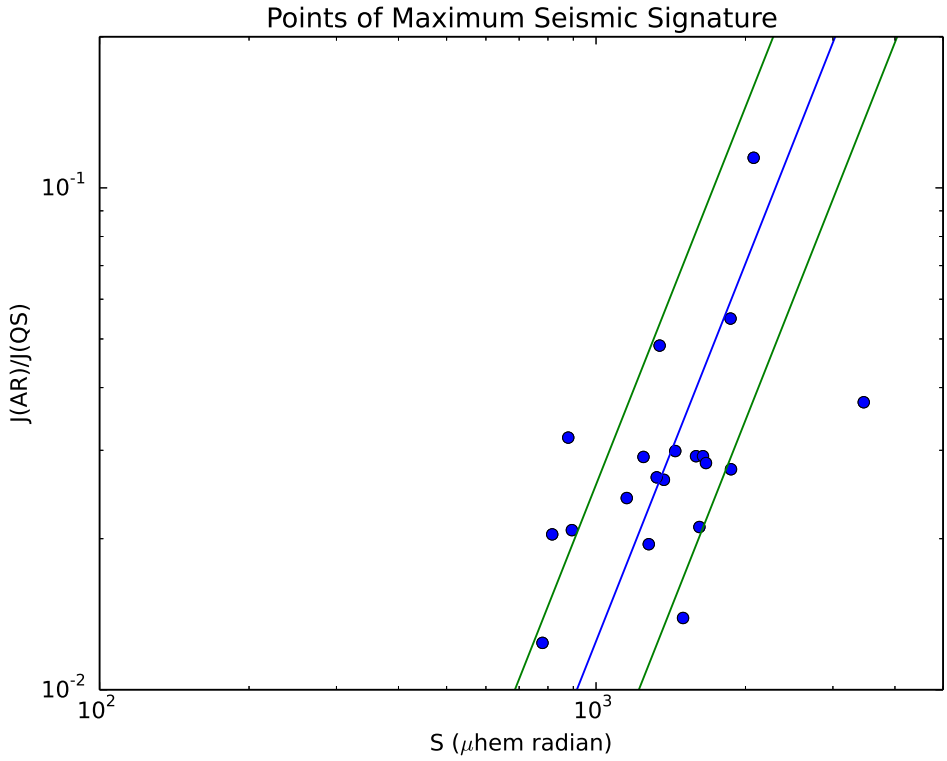

Figure 6. The brightness, J, normalized to unity for a quiet solar hemisphere (ordinate) and seismic strength, S, (abscissa) for the 22 active regions whose seismic signatures were clearly detectable during Intervals 1 and 2 are plotted at the moments where their seismic signatures were at their maxima. The diagonal blue line represents the fit expressed by equations (1) and (2). The parallel green lines delimit the corrider within the mean square deviation of the fit.

The overall statistical model suggested is that active regions become bright in HeI 304-Å relatively early in their evolution when they are still compact. Their seismic signatures then grow, as the region spreads to a greater area, and tend to decay while their EUV signatures are considerable. Figure 7 attempts to show this with trajectories that include only the starting point (green), the maximum (blue) and the end (red) of each locus.

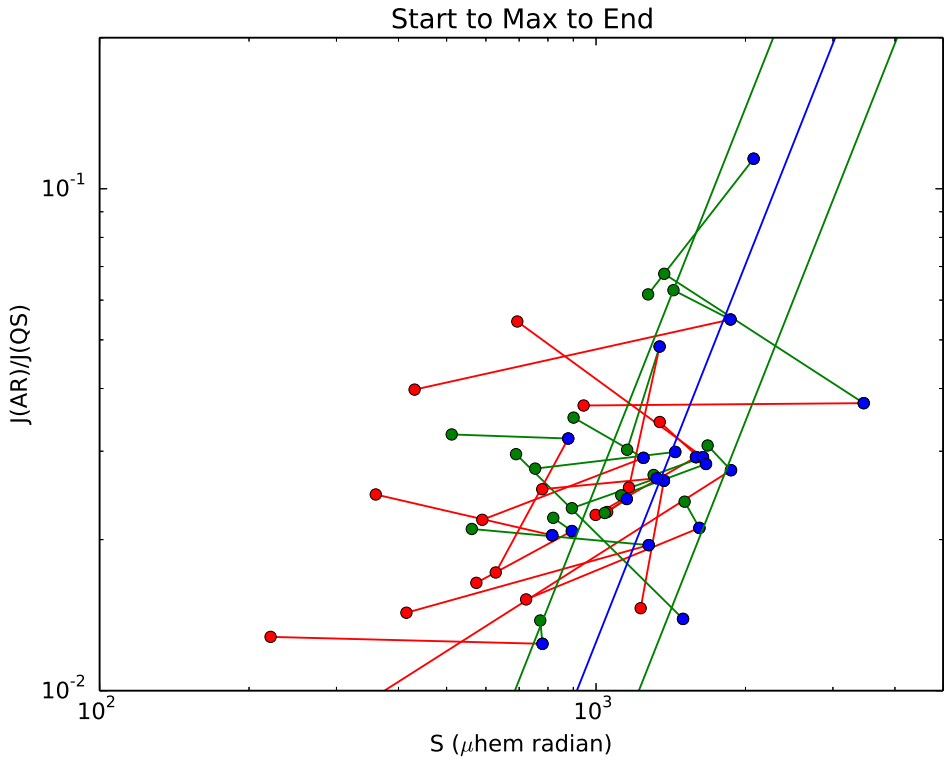

Figure 7. The trajectories connecting just the starting point, the point at which S reaches its maximum value, and the end point in the far hemisphere of each of the active regions whose seismic signatures were clearly detectable during Intervals 1 and 2 are plotted, with brightness, J, indicated by displacement in the ordinate direction and seismic strength, S, indicated by displacement in the direction of the abscissa. The starting points are colored green, the end points red, and the points at seismic maxima are rendered in blue.